Check for updates

Nitrogen self-doped activated carbons *via* the direct activation of *Samanea saman* leaves for high energy density supercapacitors†

Vichuda Sattayarut, [ID] [a] Thanthamrong Wanchaem, [ID] [a] Pundita Ukkakimapan, [ID] [a] Visittapong Yordsri, [ID] [b] Paweena Dulyaseree, [ID] [c] Mayuree Phonyiem, [ID] [a] Michiko Obata, [d] Masatsugu Fujishige, [d] Kenji Takeuchi, *[d] Winadda Wongwiriyapan [ID] *[a] and Morinobu Endo [d]

In this study, nitrogen self-doped activated carbons (ACs) obtained *via* the direct activation of *Samanea saman* green leaves (SSLs) for high energy density supercapacitors were investigated. The SSL-derived direct-activated carbons (hereinafter referred to SD-ACs) were synthesized by impregnating sodium hydroxide as an activating agent and heating up to 720 °C without a hydrothermal carbonization or pyrolysis step. The optimum condition was investigated by varying the weight ratio of raw SSLs to NaOH. Surpassing the ACs derived from the two-step convention method, SD-ACs showed superior properties, including a higher surface area (2930 m^2 g^{-1}), total pore volume (1.37 cm^3 g^{-1}) and nitrogen content (4.6 at%). Moreover, SD-ACs exhibited enhanced electrochemical properties with specific gravimetric and volumetric capacitances of 179 F g^{-1} and 88 F cm^{-3} in an organic electrolyte, respectively, a high capacitance retention of approximately 87% at a current density of 0.5 A g^{-1} and excellent cycling stability of 97.5% after 3000 cycles at a current density of 5 A g^{-1}. Moreover, the potential window of the supercapacitor cell was extended to 3.5 V with a significantly enhanced energy density of up to 79 W h kg^{-1}. These results demonstrate that the direct activation of nitrogen-enriched SSLs offers advantages in terms of simplicity, low-cost and sustainable synthetic route to achieve nitrogen self-doped ACs for high energy density supercapacitors, which exhibit superior properties to that of ACs prepared *via* the conventional method.

1 Introduction

Activated carbon (AC) is known as a high specific surface area carbon material with a hierarchical porous structure.[1,2] Recently, ACs have played a crucial role in developing green energy storage devices to overcome the crisis of global warming and the finite availability of fossil fuels. Supercapacitors or electrochemical capacitors are one of these pivotal energy storage devices, possessing outstanding advantages, including high power density, rapid charge–discharge rates, excellent stability, long cycle life and environment-friendly.[3–5] The three

main parts of supercapacitors are (i) two electrodes to adsorb and store ions, which are mainly carbon materials, (ii) a separator, which prevents the electrodes from shorting together and (iii) an electrolyte containing free mobile ions. According to the mechanism of how energy is stored, there are three types of supercapacitors: (i) electrical double-layer capacitor (EDLC), which stores energy *via* ion adsorption and formation of a charge layer *via* electrostatic interactions, (ii) pseudocapacitor using fast surface redox reactions, and (iii) hybrid supercapacitor incorporating the combination of EDLC and pseudocapacitor.[6] Hence, ACs have attracted significant scientific interest as electrode materials for all types of supercapacitors, particularly the EDLC type due to their high surface area, and good chemical and electrochemical stabilities.[7] However, there is a trade-off between their surface area and electrical conductivity due to their interconnected microporous structure, limiting the performance of ACs in supercapacitors. Therefore, great efforts have been devoted to improving the capacitive performance of ACs by functionalization *via* heteroatom doping, such as nitrogen, sulphur and oxygen.[8–18]

Heteroatom-containing functional groups have been considered to be capable of inducing pseudocapacitance,

*College of Nanotechnology, King Mongkut's Institute of Technology Ladkrabang, Chalongkrung Rd., Ladkrabang, Bangkok 10520, Thailand. E-mail: winadda.wo@kmitl.ac.th

*Thailand National Metal and Materials Technology Center, Phahonyothin Rd., Khlong Luang, Pathumthani 12120, Thailand

*Department of Physics, Faculty of Science Technology and Agriculture, Yala Rajabhat University, 133 Thesaban 3, Sateng, Muang, Yala, 95000, Thailand

*Institute of Carbon Science and Technology, Shinshu University, 4-17-1 Wakasato, Nagano, 380-8553, Japan. E-mail: takeuchi@endomoribu.shinshu-u.ac.jp

† Electronic supplementary information (ESI) available. See DOI: 10.1039/c9ra03437d

enhanced wettability of pore walls and increased conductivity in ACs. Thus, several strategies have been proposed to introduce heteroatoms into ACs, including *in situ* doping and post-processing procedures. Recently, the development of relatively simple and cost-effective strategies to synthesize ACs with excellent structural and functional properties is highly demanded and challenging. *In situ* doping using heteroatom-enriched biomass as a precursor has attracted great interest since it is a renewable, abundant and environmentally friendly resource. Normally, the conventional preparation of ACs consists of two steps: (i) carbonization step for the conversion of biomass to carbonaceous material by applying a pyrolysis or hydrothermal treatment (HTC) at a low temperature and then, (ii) activation step for the conversion of carbonaceous matter to ACs using chemical or physical activation at a high temperature. For example, nitrogen self-doped ACs are successfully prepared from nitrogen-enriched biomass waste, such as silkworm pupae, tobacco rods, wheat bran, green leaves, paper pulp and silkworm cocoons.[19–24] However, the nitrogen content in the ACs drastically decreased after activation. Moreover, the two-step conventional process is time-consuming and requires stringent reaction conditions. Thus, simple methods with low-cost and sustainable raw materials are desirable.

Currently, a simplified synthetic process that negates the need for pyrolysis or HTC has been proposed. The direct activation of biomass waste, such as seaweed, rice husks, coconut shells and onion husks, affords ACs with excellent structural and functional properties comparable to that obtained *via* the two-step route.[25–28] *Samanea saman*, the so-called rain tree, is a very large shady tree commonly cultivated as a street tree and in parks throughout tropical regions, including Thailand.[29] *Samanea saman* is also well-known as a nitrogen-fixing tree, and thus is an excellent prospect for agroforestry programs, providing a good solution to soil fertility problems. Besides its agroforestry benefits, the *Samanea saman* leaf (SSL) is considered a promising candidate as a starting precursor for nitrogen-enriched ACs. Well-known chemical agents, such as acids (HNO_3, H_2SO_4, and H_3PO_4), salts ($ZnCl_2$) and alkaline metal hydroxide (NaOH, KOH) are used to activate carbon, resulting in a high surface area and appropriate porous structure. However, activation with H_3PO_4 leads to corrosion problems with the equipment. One drawback of activation with $ZnCl_2$ is that the active carbon is contaminated with zinc salts, which are difficult to remove. Recently, it was found that molten salt is a promising chemical activating agent to develop activated carbon derived from biomass since the salt can be easily eliminated from the product and is environmentally friendly.[30] Among the chemical agents, alkaline metal hydroxide activation has resulted in predominantly microporous carbon, which is responsible for high surface area, with a narrow pore distribution and an exceptionally high total pore volume.[22,31–34] Compared to $ZnCl_2$, alkaline metal hydroxide is also beneficial in terms of its low-cost.

In this study, a high energy density supercapacitor was proposed *via* the direct activation of fresh SSLs to nitrogen self-doped ACs. The ACs derived from SSLs by direct activation (hereinafter referred to SD-AC) were synthesized by mixing them with sodium hydroxide (NaOH) as an activating agent and heating up to 720 °C. The optimum condition was investigated by varying the weight ratio of raw SSLs and NaOH. The surface area, pore volume, pore diameter and nitrogen content increased with an increase in the ratio of NaOH. Surpassing the ACs derived from SSLs *via* a two-step method (hereinafter referred to as S-AC), the SD-AC prepared with the weight ratio of SSLs to NaOH of 1 : 2 showed a higher surface area of 2930 m² g⁻¹, nitrogen content of 4.6 at%, and specific gravimetric and volumetric capacitances of 179 F g⁻¹ and 88 F cm⁻³ in organic electrolyte, respectively. Moreover, their potential window could be extended to 3.5 V with a significantly enhanced energy density of 79 W h kg⁻¹.

2 Materials and methods

2.1 Activated carbon preparation

Fresh *Samanea saman* leaves (SSLs) selected from a local plantation in Thailand were blended into small pieces after drying, and then sieved using a mesh size of 1 mm. The SSL powder was mixed with 1 M sulfuric acid (H_2SO_4) solution and stirred for 3 h at 100 °C to remove inorganic elements, such as magnesium (as shown in Fig. S1†). The mixture was then washed using deionized (DI) water until a pH of 7 was obtained and dried at 120 °C overnight. To obtain activated carbon derived from SSL by direct activation (hereinafter referred to SD-AC), the SSL powder was impregnated with NaOH at different ratios of 1 : 1.5, 1 : 1.75 and 1 : 2 (hereinafter referred to as SD1.5, SD1.75 and SD2, respectively), where *x* of SD*x* refers to the mass ratio of NaOH. The activation was conducted at 720 °C at a heating rate of 5 °C min⁻¹ for 1 h under an argon (99.999%) atmosphere at a flow rate of 500 mL min⁻¹. After activation, the sample was washed again with DI water until it reached a natural pH. A schematic of the process is shown in Fig. 1. For comparison, activated carbon derived from SSL was also prepared *via* a conventional process (hereinafter referred to as S-AC), as described elsewhere.[22,34] Briefly, prior to chemical activation, SSL was carbonized at 600 °C at a heating rate of 5 °C min⁻¹ for 2 h under nitrogen (99.999%) atmosphere to obtain charcoal. Then, the charcoal was mixed with NaOH at a weight ratio of 1 : 2.5, and subsequently activated under the same conditions as SD-ACs.

2.2 Characterizations of activated carbon

The morphological, elemental and chemical composition, and structure of the ACs were characterized using field emission scanning electron microscopy (FE-SEM, JEOL JSM-700F), X-ray photoelectron spectroscopy (XPS, PHI Quantera II) and Raman spectroscopy with a laser wavelength of 532 nm (Thermo Scientific DXR SmartRaman), respectively. Nitrogen adsorption–desorption isotherm measurements were performed by degassing at 350 °C for 12 h using a gas adsorption analyzer (Micromeritics ASAP 2020). The Brunauer–Emmett–Teller (BET) surface area was analyzed from the nitrogen adsorption isotherms, while the pore size distribution and pore volume were calculated *via* the density functional theory (DFT)
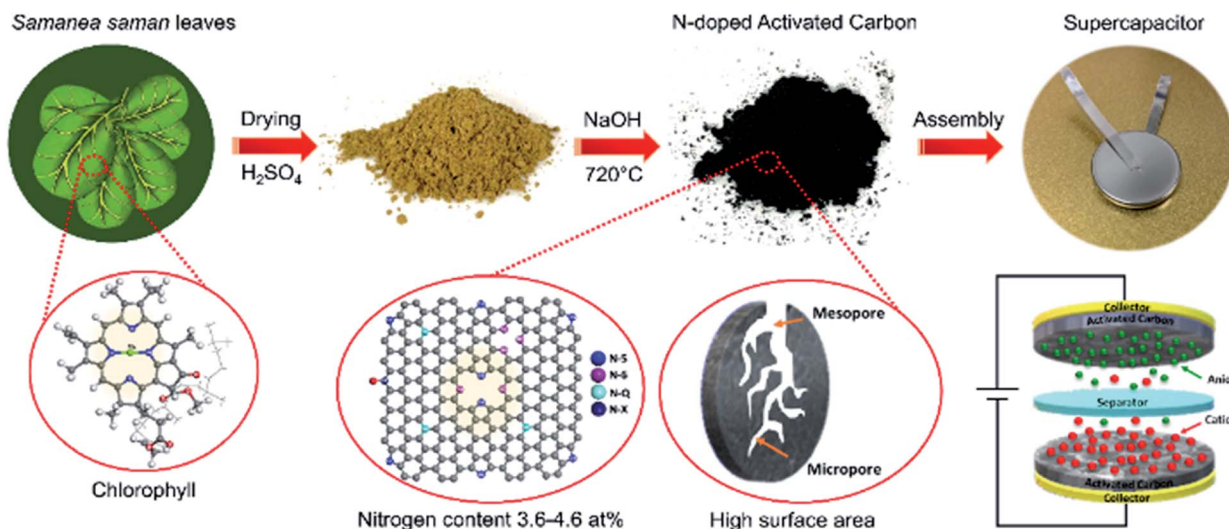
Fig. 1 Schematic of the experimental process: direct activation of SSLs to coin cell assembly.

method. The Hall effect measurement was utilized to characterize the carrier density of ACs using van der Pauw method, employing a four-point probe under a magnetic field of 0.2 T with a sample dimension of 10 mm diameter and 0.3 mm thickness (KEITHLEY 6221 DC and AC current source and 2182 NANOVOLTMETER).

2.3 Electrode preparation and characterization of electrochemical performance

The ACs were prepared as electrode pellets and assembled in a coin-cell structure for characterizing its electrochemical properties. The electrode pellets were formed as described elsewhere.[19,22] First, 90 mg of the AC was mixed with 5 mg of carbon black (CB) and 5 mg of polytetrafluoroethylene (PTFE). An electrode pellet was formed by pressing the mixture using a 10 mm diameter mold under a pressure of 10 kN. Two electrode pellets were assembled in a coin-cell structure using 1 M tetraethylammonium tetrafluoroborate (TEABF$_4$) in propylene carbonate (PC) as an electrolyte. The electrochemical properties of the electrode material and cell were characterized by cyclic voltammetry (CV), galvanostatic charge–discharge (CD), and electrochemical impedance spectroscopy (EIS). The CV test was performed in the potential range of 0.0–2.5 V with a voltage scan rate of 1 mV s^{-1}, while the CD test was set at a current density of 0.02 A g^{-1}. The specific capacitance was calculated from the CD curves using the following equation:

$$C_S = \frac{4 \times I \times \Delta t}{\Delta V \times m} \tag{1}$$

where C_S is the specific capacitance of the electrode material (F g^{-1}), I is the applied current (A), Δt is the discharge time (s), ΔV is the discharge voltage (V) and m is the weight of the electrode pellet (g). In the case of the specific capacitance of the cell (C_{cell}), C_S was further divided by four. The energy density (E, W h kg^{-1}) and power density (P, W kg^{-1}) of the device were calculated according to eqn (2) and (3), respectively.

$$E = \frac{1}{2} \times \frac{C_S}{4} \times \Delta V^2 \times \frac{1}{3.6} \tag{2}$$

$$P = \frac{E}{\Delta t} \times 3600 \tag{3}$$

3 Results and discussion

3.1 Morphology and structure characterization

Fig. 2a and b illustrate the SEM images of SD2 and S-AC at low magnification and Fig. 2c–f contain the SEM images of SD1.5, SD1.75, SD2 and S-AC at high magnification, respectively. There are no obvious differences in the morphologies between the SD- and S-ACs. At low magnification, both SD- and S-ACs show sponge-like structures. The high-magnification SEM images reveal surface roughness with small flake-like pores lower than 100 nm in size formed on the surface of the SD- and S-ACs. These pores were formed from the optimized chemical reaction of NaOH during the activation process. NaOH was decomposed into sodium during the activation process, as shown in eqn (4). The formation of pores in the carbon network by NaOH activation is related to a series of chemical reactions and Na intercalation. It is assumed that metallic sodium formed during the gasification process, which diffused into the internal structure of the carbon matrix, thus widening existing pores and creating new pores.[31]

$$6NaOH + 2C \rightarrow 2Na + 3H_2 + 2Na_2CO_3 \tag{4}$$

The morphologies from the FE-SEM images were limited to classify the porous structures. Thus, the details of the porosities of the ACs were further investigated using nitrogen adsorption–desorption isotherms. Fig. 3a shows the isotherms of the SD- and S-ACs, revealing a steep curve at the low-pressure range, then parallel to the relative pressure axis at the high-pressure
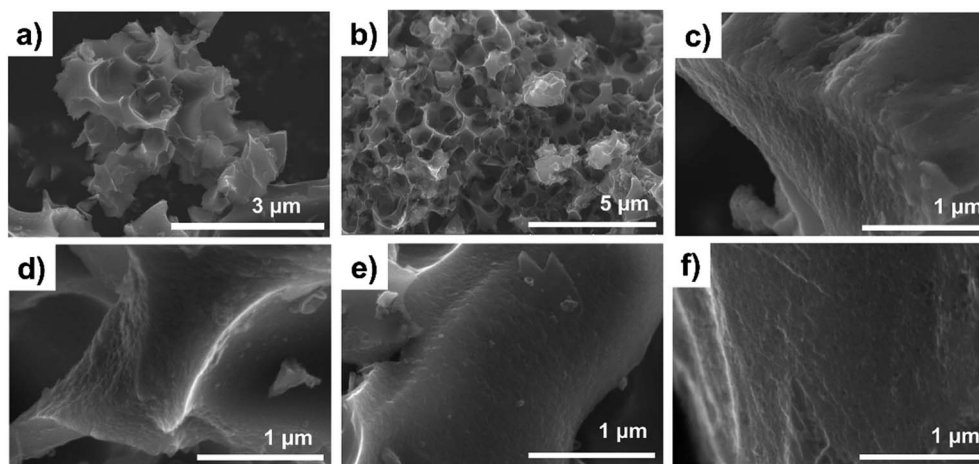
Fig. 2 SEM images at low magnification of (a) SD2 and (b) S-AC. SEM images at high magnification of (c) SD1.5, (d) SD1.75, (e) SD2 and (f) S-AC.
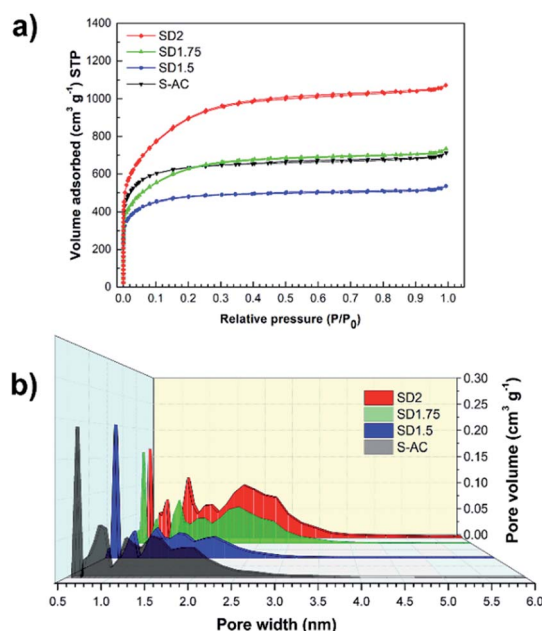

Fig. 3 (a) Nitrogen adsorption and desorption isotherms at 77 K, and (b) pore size distribution of SD1.5, SD1.75, SD2 and S-AC.

range. Hence, the SD- and S-ACs were identified as Type I isotherms (according to the IUPAC classification[35]), implying a microporous structure. A larger adsorption volume implies a larger surface area. The porosities of the SD- and S-ACs are summarized in Table 1. Among the SD-ACs, SD2 showed the highest surface area and the highest total pore volume.

Compared to S-AC, the specific surface area (S_{BET}) of SD2 increased from 2403 to 2930 m^2 g^{-1}, and the total pore volume (V_{total}) increased from 0.86 to 1.37 cm^3 g^{-1}. Furthermore, the adsorption–desorption isotherm of SD1.5 exhibited a sharp knee at the relative low pressure region ($P/P_0 < 0.1$) and a long plateau, implying a narrow micropore distribution, while that of SD1.75 and SD2 exhibited a gradually wider curve before a long plateau, implying a wider micropore distribution. These are evident in the pore size distributions, as shown in Fig. 3b, which were calculated using the DFT method. These results show that increasing the mass ratio of NaOH provides a sustained increase in S_{BET} and pore volume. However, under our experimental conditions, the maximum mass ratio of NaOH was limited in SD2. The excess NaOH molecules deposited in the carbon pore wall might have caused catalytic oxidation and decomposition, reducing the adsorption uptake and carbon yield, as shown in eqn (5):[31,36]

$$4NaOH + C \rightarrow 4Na + CO_2 + 2H_2O \tag{5}$$

Compared to that from the conventional activation, SD2 showed superior properties in surface area (2930 > 2403 m^2 g^{-1}), total pore volume (1.37 > 0.86 cm^3 g^{-1}), volume ratio of mesopores and total pores (V_{meso}/V_{total}) (0.35 > 0.11) and pore size (1.72 > 1.63 nm), implying that the direct activation is a suitable

Table 1 Porosity properties of SD- and S-ACs from N$_2$ adsorption–desorption isotherms

Sample	S_{BET}^{a} (m^2 g^{-1})	Pore diameter^b (nm)	V_{total}^{c} (cm^3 g^{-1})	V_{micro}^{d} (cm^3 g^{-1})	V_{meso}^{d} (cm^3 g^{-1})	V_{micro}/V_{total}	V_{meso}/V_{total}
S-AC	2403	1.63	0.86	0.75	0.10	0.87	0.11
SD1.5	1790	1.64	0.67	0.58	0.09	0.87	0.13
SD1.75	2112	1.72	0.92	0.65	0.27	0.71	0.29
SD2	2930	1.72	1.37	0.89	0.48	0.65	0.35

^{a} BET (Brunauer–Emmett–Teller) surface area. ^{b} Pore diameter from DA method. ^{c} Total pore volume from DFT method. ^{d} Micropore–mesopore volume from DFT method.

method for mesopore development and pore expansion, even though a lower NaOH mass ratio is used. The existence of mesopores and wide pore diameter of the ACs played an important role as a convenient route for the transportation and penetration of electrolyte ions, which lead to fast ion transfer.[37] The significant increase in surface area for SD2 compared that of S-ACs may be attributed to the synergistic effect of the organic matter decomposition and NaOH chemical activation.

Raman spectra of SD- and S-ACs are shown in Fig. 4. A pair overlapping relatively broad peaks, which are commonly known as the D-band and G-band, were observed at approximately 1360 cm^{-1} and 1600 cm^{-1}, respectively. The D-band originated from defects and disordered carbon structures, while the G-band originated from the graphitic structure. The intensity ratio of the D-band to G-band (I_D/I_G) is proportional to the ratio of defect sites in carbon materials.[38,39] The value of I_D/I_G tend to decrease when the chemical impregnation ratio increased (SD1.5 (0.99) > SD1.75 (0.98) > SD2 (0.97)). This indicates that at a higher NaOH content in direct activation, the amorphous structures and organic components decomposed, resulting in a higher degree of graphitic structures. However, S-AC showed a lower I_D/I_G (0.94) compared to SD-ACs. In the case of conventional activation, the sample is thermally treated during the carbonization and activation steps, thus improving the graphitic degree. Besides, ACs with a lower surface area can maintain their carbon network, resulting in a high graphitic structural alignment. However, a degree of graphitic carbon structure and heteroatom content are necessary to obtain the optimum electrochemical properties. Moreover, the XRD patterns of each sample exhibited two broad peaks at approximately 24.0° and 44.6°, corresponding to the (002) and (100) planes, respectively (as shown in Fig. S2†). A broad shape with a low intensity of diffraction peak implies a disordered carbon structure and amorphous carbon.

The XPS technique was utilized to investigate the elemental composition and their chemical states of the ACs. The quantitative analysis of the elemental composition is summarized in Table 2. The ACs consisted of carbon, oxygen and nitrogen. The carbon contents in SD1.5, SD1.75, SD2 and S-AC were 86.7, 87.6, 88.40 and 90.6 at%, respectively. C=C is the dominant

Table 2 XPS peak analysis of SD- and S-ACs

Sample	Content (at%)			N/C ratio (%)	Relative N1s peak area^a (at%)			
	C	O	N		N-6	N-5	N-Q	N-X
S-AC	90.6	7.7	1.7	1.82	0.41	0.72	0.40	0.17
SD1.5	86.7	9.7	3.6	4.15	0.87	1.98	0.58	0.17
SD1.75	87.6	8.2	4.2	4.79	1.03	2.34	0.72	0.11
SD2	88.4	7.0	4.6	5.20	1.10	2.58	0.87	0.05

^{a} Pyridine N (N-6), pyrrolic N (N-5), quaternary N (N-Q) and oxidized pyridine N (N-X).

component in all samples (Fig. S3 and Table S2†). The higher graphitic carbon content in S-AC than that in SD-ACs is consistent with the I_D/I_G results from the Raman spectra. Moreover, the nitrogen-enriched ACs play a pivotal role in improving the electrical conductivity and pseudo-capacitance of supercapacitors.[8–10,40]

The nitrogen contents in SD1.5, SD1.75, SD2 and S-AC are 3.6, 4.2, 4.6 and 1.7 at%, respectively. The nitrogen content in SD2 was approximately 3 times higher than that in S-AC. The ratios of nitrogen and carbon (N/C ratio) followed the order: S-AC (1.8%) < SD1.5 (4.1%) < SD1.75 (4.8%) < SD2 (5.2%). Moreover, compared to the carbonized S-ACs, the nitrogen content in S-AC after activation decreased from 2.2 at% to 1.7 at%. During carbonization at 600 °C for 2 h, chlorophyll may be decomposed with other organic compounds, resulting in a decrease in the nitrogen content. The source of nitrogen in SSLs may come from chlorophyll, which is related to green pigments found in the chloroplasts of plants, providing nitrogen self-doped ACs.[41,42] It was found that the main elemental composition of SSLs were carbon, nitrogen, oxygen, magnesium and sulfur (as shown in Fig. S1 and Table S1†). Interestingly, the atomic ratio of nitrogen to magnesium is approximately 3.6, corresponding to the molecular structure of chlorophyll, which is four pyrrole rings containing nitrogen arranged in a ring around a magnesium ion, and a long hydrocarbon tail.[43] Moreover, the nitrogen content in the SSL-derived activated carbon is approximately 4.6 at%. This value is comparable to the nitrogen-doped mesoporous by post treatment under an ammonia atmosphere, which included approximately 2.96–7.8 at% nitrogen.[17,18,44,45] These results imply that the direct activation of nitrogen-containing agricultural waste, such as SSLs, is a promising approach to obtain nitrogen self-doped activated carbon.

The N1s spectra were further deconvoluted to analyze their nitrogenated structures, as shown in Fig. 5. There are four main peaks of nitrogen in different chemical states in the carbon network located at approximately 398.3, 399.8, 401.1 and 403.6 eV, corresponding to pyridinic nitrogen (N-6), pyrrolic nitrogen (N-5), quaternary nitrogen (N-Q) and oxidized nitrogen (N-X), respectively.[8–10,46,47] The content of each nitrogenated structure was calculated based on the peak area, as shown in Table 2. Interestingly, N-5 was the main component of all the samples, while other nitrogen configurations were in the following order: N-6 > N-Q > N-X. The origin of the dominant N-
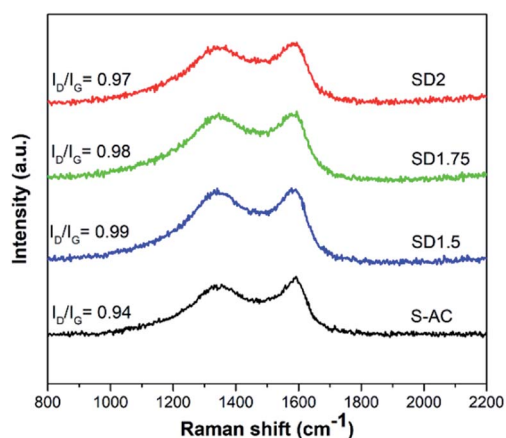

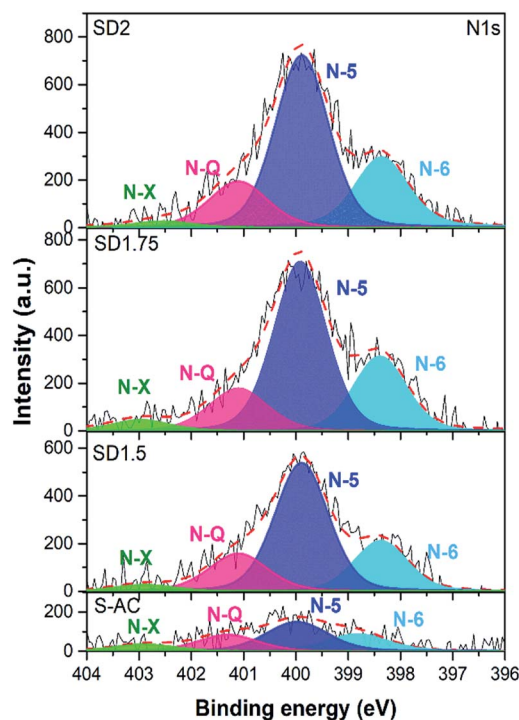**Fig. 4** Raman spectra of SD- and S-ACs.

Fig. 5 XPS spectra of SD- and S-ACs.

5 is depicted from the structure of chlorophyll, which consists of a porphyrin head, *i.e.* four pyrrole rings containing nitrogen arranged in a ring around a magnesium ion, and a long hydrocarbon tail.[43] In general, N-5 and N-6 bond with two sp[2] carbon atoms and contribute electron lone pairs to the carbon conjugated systems, consequently inducing electron donor and chemical reactivity of the carbon atoms, and playing a prominent role in the pseudocapacitance behavior. In the case of N-Q, the nitrogen atom takes the position inside an aromatic ring (so-called graphitic N) with sp[2] hybridization and saturated bonding, enhancing the electrical conductivity of carbon materials.[22,40] Since it is theoretically proven that the nitrogen acts as an electron donor in the carbon networks, the Hall effect measurement was employed to investigate the electrical properties of the ACs. The calculated resistivity and charge density of SD2 and S-AC were approximately 0.78 Ω cm and 1.09×10^{19} cm^{-3}, and 0.82 Ω cm and 5.03×10^{18} cm^{-3}, respectively. The lower resistivity and higher carrier density are also evidence of a higher nitrogen doping in SD2 and are consistent with the XPS analysis results.

Furthermore, the activated carbon also included approximately 7.0–9.7 at% oxygen. The O1s spectra are deconvoluted, as shown in Fig. S4.† The oxygen-containing configurations of all the samples are classified into three groups, including O=C–OH in carboxyl groups (531.2), C=O in carbonyl groups (532.2 eV) and C–OH in phenol groups and/or C–O–C in ether groups (533.2 eV). The presence of oxygenated functional groups may improve the wettability of the carbon surface and increase the specific capacitance by taking part in a faradaic reaction.[19,48]

The productivity of the ACs derived from SSLs using the conventional method and the direct activation was

approximately 30% and 10%, respectively. Although, the direct activation showed a lower productivity, it exhibited advantages in terms of higher surface area and higher nitrogen content. Moreover, the direct activation is simple and not time-consuming. The productivity of the SSL-derived ACs is comparable to other plant-based biomass-derived ACs by the conventional method, and higher than the ACs derived from animal sources, such as silkworm pupae.[19]

3.2 Electrochemical properties in organic electrolyte

This study focused on an organic electrolyte with a cell operating voltage of up to 2.5 V due to the high demand for a wide voltage and high energy in practical application and the voltage limitation of aqueous electrolyte determined by the electrochemical breakdown of water.[3,49] In order to improve the energy density, the electrochemical performances of the ACs were assembled in a two-electrode coil cell and were evaluated in 1 M TEABF$_4$ electrolyte.

Fig. 6a shows the CV curves of all samples at a scan rate of 1 mV s^{-1} in the potential window range of 0–2.5 V. A relatively quasi-rectangular shape indicates an electrical double-layer capacitor (EDLC) at the interface between the electrode material and electrolyte. Particularly, the SD-ACs displayed an additional hump located at approximately 1.6 V generated from redox reactions of the nitrogenated functional groups,[50] while the hump was not clearly observed in S-AC due to its lower nitrogen content. Although the surface area of S-AC was higher than that of the SD1.75, the larger area of the CV curve of SD1.75 than that of the S-AC implies a high capacitance occurring from redox reaction due to nitrogenated functional groups.

Fig. 6b shows the galvanostatic CD curves at a current density of 0.02 A g^{-1} in the potential range of 0–2.5 V. All the CD curves have a symmetric triangular-type shape, presenting excellent electrochemical reversibility and supercapacitive behavior.[51] SD-ACs showed a longer charge–discharge time, indicating a higher specific capacitance than S-AC. The values of the specific gravimetric and volumetric capacitances of each electrode material were calculated from their CD curves, which showed the following order: SD2 (179.2 F g^{-1}, 87.8 F cm^{-3}) > SD1.75 (168.8 F g^{-1}, 85.5 F cm^{-3}) > SD1.5 (150.8 F g^{-1}, 76.0 F cm^{-3}) > S-AC (138.2 F g^{-1}, 75.6 F cm^{-3}). SD2 exhibited the best performance in both specific gravimetric and volumetric capacitances, which is attributed to the synergistic effects of its highest surface area and nitrogen-containing functional groups.

Fig. 6c displays the EIS spectra of all the samples in the frequency range of 0.01 Hz to 1 MHz by applying an amplitude of 5 mV. The EIS spectra consist of two main regions: first, a semicircle at the high-frequency region, which is related to the series resistance (R_S) and the charge-transfer resistance (R_{CT}), and second, a nearly vertical linear line at the low-frequency region, which corresponds to the diffusion-controlled process.[52] All the samples presented similar semicircle curves, but different x-intercepts and diameters. The x-intercept (Z' (Ω)) can be interpreted as the R_S of the electrode, which is the total resistance of the electrode material, electrolyte, and the contact resistance between the collector and electrode material. The values of R_S for SD1.5, SD1.75, SD2 and S-AC were approximately
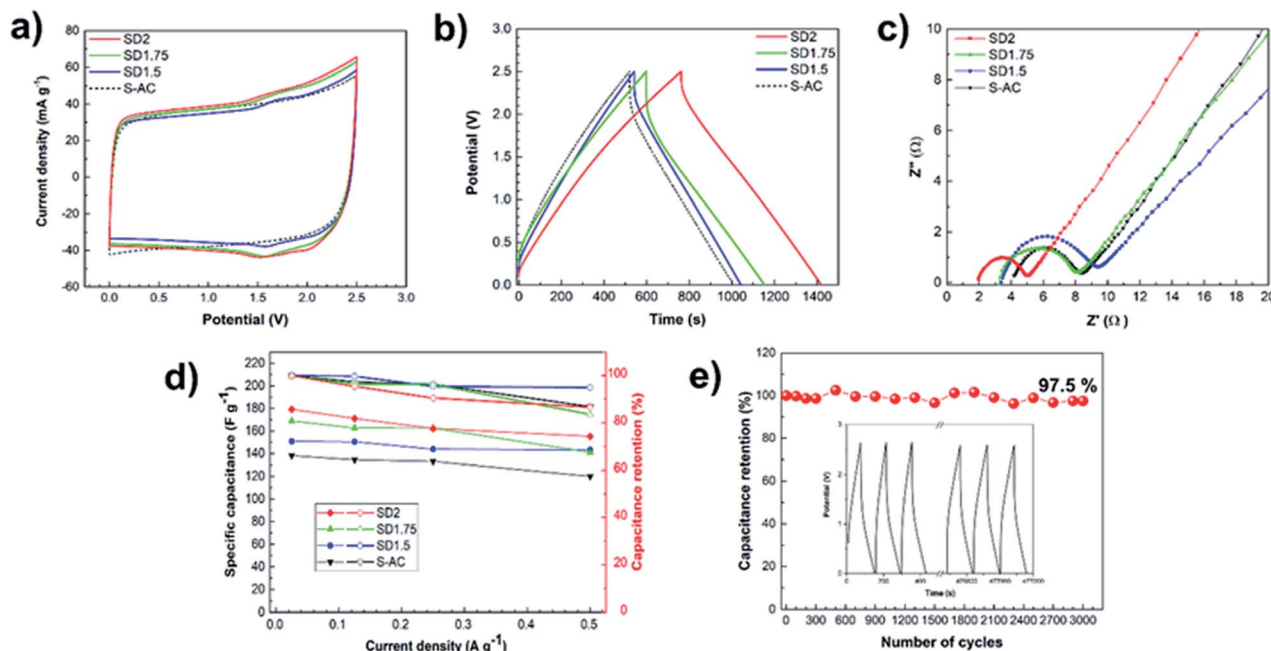
Fig. 6 Electrochemical performances of electrodes based on SD- and S-ACs measured in 1 M TEABF$_4$. (a) CV curves at a scan rate of 1 mV s^{-1}, (b) CD curves at an applied current of 0.02 A g^{-1}, (c) EIS at 0.01 Hz to 1 MHz, (d) specific capacitance at various current densities and (e) capacitance retention of SD2 at a current density of 0.5 A g^{-1}. The inset shows the CD cycles.

3.27, 3.18, 1.98 and 4.18, 3 Ω, respectively. The R_{CT} values were measured from the diameter of the semicircle, representing the kinetic resistance. The values of R_{CT} of SD1.5, SD1.75, SD2 and S-AC were approximately 6.05, 4.82, 3.07 and 4.18 Ω, respectively. SD2 showed the lowest R_S and R_{CT} compared to S-AC, implying its enhanced electrochemical properties.

Normally, the important factors for the enhancement of supercapacitor performance are surface area, mesopore volume, pore diameter and heteroatom doping in carbon materials, which can be described as follows: (i) a large surface area with a high ratio of mesopore seems to be the preferable path for ion accessibility. In an organic electrolyte, the ions involved in the capacitive behavior are in the form of desolvated and/or partially desolvated ions. The solvated ions are generally larger than the desolvated ions. The anion

tetraethylammonium (TEA$^+$) solvated and desolvated ions are 1.35 and 0.67 nm, respectively, and cation tetrafluoroborate (BF$_4^-$) are 1.40 and 0.48 nm, respectively.[53] Accordingly, the large and unstable ion size of organic electrolytes compared to that of the aqueous electrolyte makes it difficult to transfer into the micropores.[54] Hence, the enlarged volume of the mesopore and larger average pore diameter of SD-ACs provide an accessible route for ions to transfer trough the porous network, contributing to the supercapacitor enhancement in organic electrolyte system.[37] (ii) The nitrogen heteroatom in SD-ACs also plays a crucial role in improving its capacitive performance, as clearly seen in SD1.5 and SD1.75 with a larger area of CV curves, longer discharge time of CD curves and smaller x-intercept and smaller semicircle of EIS spectra. The performance improvement can be explained by the following reasons. The electron lone pair
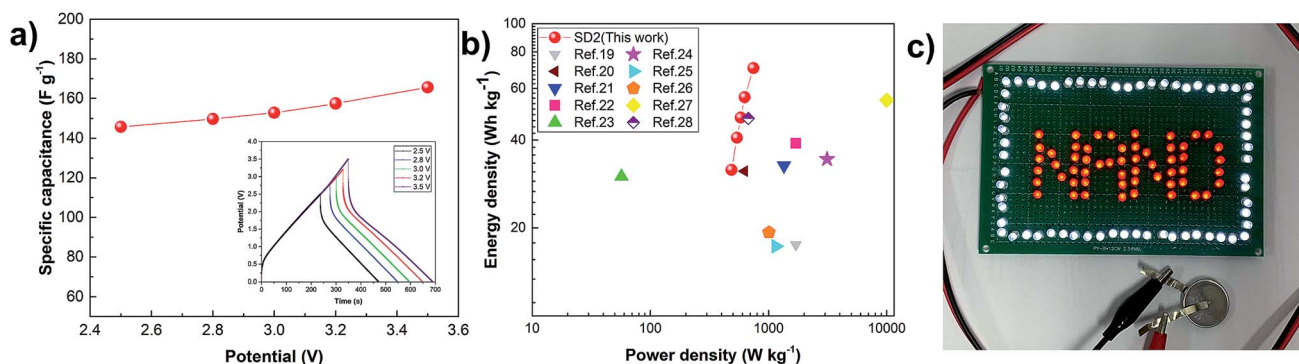

Fig. 7 Electrochemical performances of coin cell based on SD2. (a) Specific capacitance against various voltages, and the inset displays the CD curves at a current density of 0.3 A g^{-1}, (b) Ragone plot of coil cell of SD2 compared to other reports, and (c) photograph of one cell of SD2 lighting up 64 white LEDs and 54 red LEDs.

from N-5 and N-6 can enhance the electrochemical performance by inducing a faradaic reaction.[19,22] The contributing positive charge of N-Q is inside the aromatic ring (graphitic N) with sp^2 hybridization and saturated bonding, leading to an enhancement in the electrical conductivity of the carbon material.[40] This was confirmed by the result in the reduction of R_S and R_{CT} of SD2.

In addition, Fig. 6d shows the specific capacitance of each electrode applied at various current densities from 0.02 A g^{-1} to 0.5 A g^{-1}. Each sample exhibited a gradual decrease in specific capacitance when the current densities increased. SD2 had the highest specific capacitance even at a current density of 0.5 A g^{-1}. The capacitance retention of SD2 (87%) was relatively equivalent to that of S-AC (87%). Furthermore, the long-life cycling performance of the SD2-based electrode was examined *via* CD measurements at a current density of 0.5 A g^{-1}. As shown in Fig. 6e, SD2 exhibited a capacitance retention of 97.5% after 3000 cycles, suggesting the highly stable and reversible charge–discharge process of the electrode. The inset of Fig. 6e shows the CD curves of the first and last three cycles, implying excellent stable cyclic ability with unchanged triangle shapes.

3.3 Enhancement in the electrochemical properties

In order to improve the energy and power densities of the supercapacitor, the highly nitrogen-enriched SD2 was demonstrated to expand its potential window up to 3.5 V based on the TEABF$_4$ electrolyte. The CD curves were measured in the potential range of 2.5–3.5 V at an applied current density of 0.3 A g^{-1}. The specific capacitances gradually increased with potential, as shown in Fig. 7a, achieving the maximum specific gravimetric and volumetric capacitance for the electrode material of 184.7 F g^{-1} and 86.0 F cm^{-3} at the potential voltage range of 3.5 V, respectively. Moreover, the inset of Fig. 7a displays the CD curves against the potential range of 2.5–3.5 V with a triangle shape, confirming the good electrochemical reversibility and supercapacitive behavior. The small voltage drop was due to the relatively high viscosity and low conductivity of the organic electrolyte in ambient conditions.[55]

Fig. 7b shows the Ragone plot, which is a plot of power density against energy density, of the SD2 cell compared to other supercapacitor cells using green leave-derived ACs *via* conventional method and other biomass material-derived ACs *via* conventional and direct methods.[19–28] The data for each cell is summarized in Table S3.† The SD2 cell showed an energy density and power density of 35.3 W h kg^{-1} and 542.3 W kg^{-1} at 2.5 V and outstanding 78.5 W h kg^{-1} and 829.7 W kg^{-1} at 3.5 V, respectively, exhibiting an improvement in energy density compared to the ACs in other works. In addition, one of the symmetric supercapacitor cells based on SD2 was successfully used as a power source operating at 3.5 V to illuminate 64 super-bright white LEDs and 54 red LEDs, as shown in Fig. 7c.

4 Conclusions

In summary, nitrogen-enriched ACs derived *via* the direct activation of SSLs for supercapacitors with high energy density were successfully demonstrated. The SD-ACs were synthesized by mixing SSLs with NaOH and direct activation at an elevated temperature of 720 °C without a carbonization step. The optimum weight ratio of raw SSLs and NaOH was 1 : 2 (SD2), resulting in ACs with superior properties than those prepared *via* the conventional two-step method. SD2 afforded nitrogen self-doping during the direct activation of SSLs with a relatively high surface area (2930 m^2 g^{-1}), total pore volume of 1.37 cm^3 g^{-1} and nitrogen content of 4.6 at%. Moreover, SD2 exhibited the highest electrochemical performance in organic electrolyte with the gravimetric and volumetric specific capacitances of 179.2 F g^{-1} and 87.8 F cm^{-3}, respectively, and capacitance retention of 97.5% after 3000 cycles with a current density of 5 A g^{-1}. In addition, the enhanced energy density of the SD2 supercapacitor device was investigated in the voltage range of 2.5 to 3.5 V, showing the maximum energy and power densities of approximately 78.5 W h kg^{-1} and 829 W kg^{-1}, respectively, at 3.5 V. These results show that the direct activation of SSLs is an effective method in terms of simplicity, low-cost and sustainability for the synthesis of nitrogen self-doped ACs for high energy density supercapacitors.

Contributions

K. T., W. W. and M. E. designed and directed the project. V. S., P. U. and P. D. synthesized the samples. V. S., V. Y., M. O. and M. F. characterized material properties (SEM, nitrogen adsorption–desorption isotherm measurements, Raman spectroscopy, XPS). V. S., T. W. and M. P. measured electrochemical properties. K. T., M. P. and W. W. helped interpreting the results. V. S., K. T. and W. W. worked on the manuscript. All authors discussed the results and commented on the manuscript.

Conflicts of interest

There are no conflicts to declare.

Acknowledgements

References

1 J. Lee, J. Kim and T. Hyeon, *Adv. Mater.*, 2006, **18**, 2073.

2 O. Ioannidou and A. Zabaniotou, *J. Renewable Sustainable Energy*, 2007, **11**, 1966.

3 R. Kötz and M. Carlen, *Electrochim. Acta*, 2000, **45**, 2483.

4 A. Burke, *Electrochim. Acta*, 2007, **53**, 1083.

5 J. R. Miller and P. Simon, *Science*, 2008, **321**, 651.

6 E. Lim, C. Jo and J. Lee, *Nanoscale*, 2016, **8**, 7827.

7 A. M. Abioye and F. N. Ani, *J. Renewable Sustainable Energy*, 2015, **52**, 1282.

8 G. Lota, B. Grzyb, H. Machnikowska, J. Machnikowski and E. Frackowiak, *Chem. Phys. Lett.*, 2005, **404**, 53.

9 D. Hulicova-Jurcakova, M. Kodama, S. Shiraishi, H. Hatori, Z. H. Zhu and G. Q. Lu, *Adv. Funct. Mater.*, 2009, **19**, 1800.

10 D. Hulicova-Jurcakova, M. Seredych, G. Q. Lu and T. J. Bandosz, *Adv. Funct. Mater.*, 2009, **19**, 438.

11 B.-L. Xing, H. Guo, L.-J. Chen, Z.-F. Chen, C.-X. Zhang, G.-X. Huang, W. Xie and J.-L. Yu, *Fuel Process. Technol.*, 2015, **138**, 734.

12 Y. Li, G. Wang, T. Wei, Z. Fan and P. Yan, *Nano Energy*, 2016, **19**, 165.

13 D. Chen, L. Yang, J. Li and Q. Wu, *ChemistrySelect*, 2019, **4**, 1586.

14 G. Lin, R. Ma, Y. Zhou, C. Hu, M. Yang, Q. Liu, S. Kaskel and J. Wang, *J. Colloid Interface Sci.*, 2018, **527**, 230.

15 G. Lin, R. Ma, Y. Zhou, Q. Liu, X. Dong and J. Wang, *Electrochim. Acta*, 2018, **261**, 49.

16 B. Xing, R. Yuan, C. Zhang, G. Huang, H. Guo, Z. Chen, L. Chen, G. Yi, Y. Zhang and J. Yu, *Fuel Process. Technol.*, 2017, **165**, 112.

17 T. Zhou, Y. Zhou, R. Ma, Z. Zhou, G. Liu, Q. Liu, Y. Zhu and J. Wang, *Carbon*, 2017, **114**, 177.

18 T. Zhou, R. Ma, Y. Zhou, R. Xing, Q. Liu, Y. Zhu and J. Wang, *Microporous Mesoporous Mater.*, 2018, **261**, 88.

19 V. Sattayarut, C. Chanthad, P. Khemthong, S. Kuboon, T. Wanchaem, M. Phonyiem, M. Obata, M. Fujishige, K. Takeuchi, W. Wongwiriyapan, P. Khanchaitit and M. Endo, *RSC Adv.*, 2019, **9**, 9878.

20 Y.-Q. Zhao, M. Lu, P.-Y. Tao, Y.-J. Zhang, X.-T. Gong, Z. Yang, G.-Q. Zhang and H.-L. Li, *J. Power Sources*, 2016, **307**, 391.

21 D. Wang, Y. Min and Y. Yu, *J. Solid State Electrochem.*, 2015, **19**, 577.

22 P. Dulyaseree, M. Fujishige, I. Yoshida, Y. Toya, Y. Banba, Y.-s. Tanaka, T. Aoyama, M. Phonyiem, W. Wongwiriyapan, K. Takeuchi and M. Endo, *RSC Adv.*, 2017, **7**, 42064.

23 H. Wang, Z. Li, J. K. Tak, C. M. B. Holt, X. Tan, Z. Xu, B. S. Amirkhiz, D. Harfield, A. Anyia, T. Stephenson and D. Mitlin, *Carbon*, 2013, **57**, 317.

24 J. Sun, J. Niu, M. Liu, J. Ji, M. Dou and F. Wang, *Appl. Surf. Sci.*, 2018, **427**, 807.

25 E. Raymundo-Piñero, M. Cadek and F. Béguin, *Adv. Funct. Mater.*, 2009, **19**, 1032.

26 X. He, P. Ling, J. Qiu, M. Yu, X. Zhang, C. Yu and M. Zheng, *J. Power Sources*, 2013, **240**, 109.

27 L. Sun, C. Tian, M. Li, X. Meng, L. Wang, R. Wang, J. Yin and H. Fu, *J. Mater. Chem. A*, 2013, **1**, 6462.

28 D. Wang, S. Liu, G. Fang, G. Geng and J. Ma, *Electrochim. Acta*, 2016, **216**, 405.

29 P. A. Durr, *Agroforestry Systems*, 2001, **51**, 223.

30 P. Chen, S. Lu, C. Yang, Z. He, X. Chen and K. Guo, *Energy Technol.*, 2018, **6**, 2273.

31 M. A. Lillo-Ródenas, D. Cazorla-Amorós and A. Linares-Solano, *Carbon*, 2003, **41**, 267.

32 L. Khezami, A. Ould-Dris and R. Capart, *BioResources*, 2007, **2**, 193.

33 T. Kawano, M. Kubota, M. Onyango, F. Watanabe and H. Matsuda, *Appl. Therm. Eng.*, 2008, **28**, 865.

34 K. Takeuchi, M. Fujishige, N. Ishida, Y. Kunieda, Y. Kato, Y. Tanaka, T. Ochi, H. Shirotori, Y. Uzuhashi, S. Ito, K.-i. Oshida and M. Endo, *J. Phys. Chem. Solids*, 2018, **118**, 137.

35 M. Thommes, K. Kaneko, A. V. Neimark, J. P. Olivier, F. Rodriguez-Reinoso, J. Rouquerol and K. S. W. Sing, *Pure Appl. Chem.*, 2015, **87**, 9.

36 M. A. Lillo-Ródenas, J. Juan-Juan, D. Cazorla-Amorós and A. Linares-Solano, *Carbon*, 2004, **42**, 1371.

37 A. G. Pandolfo and A. F. Hollenkamp, *J. Power Sources*, 2006, **157**, 11.

38 M. W. Smith, I. Dallmeyer, T. J. Johnson, C. S. Brauer, J.-S. McEwen, J. F. Espinal and M. Garcia-Perez, *Carbon*, 2016, **100**, 678.

39 C. Guizani, K. Haddad, L. Limousy and M. Jeguirim, *Carbon*, 2017, **119**, 519.

40 M. Yang and Z. Zhou, *Adv. Sci.*, 2017, **4**, 1600408.

41 H. Chen, F. Yu, G. Wang, L. Chen, B. Dai and S. Peng, *ACS Omega*, 2018, **3**, 4724.

42 C. Ragasa, R. Galian, M. Arenal, V. Tan and c.-c. Shen, *Res. J. Pharm., Biol. Chem. Sci.*, 2014, **5**, 1501.

43 B. H. Patel, in *Handbook of Textile and Industrial Dyeing*, ed. M. Clark, Woodhead Publishing, Kidlington, United Kingdom, 2011, vol. 1, ch. 11 – Natural dyes, p. 395.

44 D. Gu, Y. Zhou, R. Ma, F. Wang, Q. Liu and J. Wang, *Nano-Micro Lett.*, 2017, **10**, 29.

45 R. Xing, T. Zhou, Y. Zhou, R. Ma, Q. Liu, J. Luo and J. Wang, *Nano-Micro Lett.*, 2017, **10**, 3.

46 H. Schmiers, J. Friebel, P. Streubel, R. Hesse and R. Köpsel, *Carbon*, 1999, **37**, 1965.

47 R. Wang, T. Zhou, H. Li, H. Wang, H. Feng, J. Goh and S. Ji, *J. Power Sources*, 2014, **261**, 238.

48 F. Zeng, Z. Li, X. Li, J. Wang, Z. Kong, Y. Sun, Z. Liu and H. Feng, *Appl. Surf. Sci.*, 2019, **467–468**, 229.

49 M. Frank Rose, C. Johnson, T. Owens and B. Stephens, *J. Power Sources*, 1994, **47**, 303.

50 X. Chen, J. Zhang, B. Zhang, S. Dong, X. Guo, X. Mu and B. Fei, *Sci. Rep.*, 2017, **7**, 7362.

51 T. Wei, Q. Zhang, X. Wei, Y. Gao and H. Li, *Sci. Rep.*, 2016, **6**, 22646.

52 K. Karthikeyan, S. Amaresh, S. N. Lee, X. Sun, V. Aravindan, Y.-G. Lee and Y. S. Lee, *ChemSusChem*, 2014, **7**, 1435.

53 C.-M. Yang, Y.-J. Kim, M. Endo, H. Kanoh, M. Yudasaka, S. Iijima and K. Kaneko, *J. Am. Chem. Soc.*, 2007, **129**, 20.

54 J. Chmiola, G. Yushin, Y. Gogotsi, C. Portet, P. Simon and P. L. Taberna, *Science*, 2006, **313**, 1760.

55 P. Liu, M. Verbrugge and S. Soukiazian, *J. Power Sources*, 2006, **156**, 712.